Efficiencies for production of atomic nitrogen and oxygen by relativistic proton impact in air

H. S. Porter, C. H. Jackman, and A. E. S. Green

University of Florida, Gainesville, Florida 32611
(Received 5 March 1976)

Relativistic electron and proton impact cross sections are obtained and represented by analytic forms which span the energy range from threshold to 10^9 eV. For ionization processes, the Massey–Mohr continuum generalized oscillator strength surface is parametrized. Parameters are determined by simultaneous fitting to (1) empirical data, (2) the Bethe sum rule, and (3) doubly differential cross sections for ionization. Branching ratios for dissociation and predissociation from important states of N_2 and O_2 are determined. The efficiency for the production of atomic nitrogen and oxygen by protons with kinetic energy less than 1 GeV is determined using these branching ratio and cross section assignments.

I. INTRODUCTION

Recently several papers estimating the production of nitric oxide by cosmic rays have appeared.[1–3] Central to the determination of the nitric oxide produced by cosmic rays is the number and state of excitation of atomic nitrogen atoms which result during the deposition process. In previous determinations rough estimates of these quantities have been obtained. In the present paper we report a more complete determination of the production of atomic nitrogen and oxygen atoms by cosmic rays.

Our method may be described as a detailed atomic cross section approach which has evolved from the work of Green and collaborators.[4–9] In the present paper we generalize the approach to relativistic energies and define branching ratios for dissociation to give the efficiency for production of atomic nitrogen and oxygen. While the incident protons (other heavy projectiles may be treated in the Born approximation in an analogous manner) are relativistic, it is important to realize that a large fraction of this incident energy is actually deposited in the accessible states of N_2 and O_2 by secondary electrons of low energy (a few 10's of eV). Consequently, the low energy electron cross sections and the shape of the secondary electron spectrum as a function of secondary energy for a given primary energy are of considerable importance. It also should be pointed out that because of the change in shape of the secondary electron spectrum with changing primary energy, as well as the changing energy dependence of various processes, that the efficiency for the production of atomic species is a function of the local energy of the projectile at each depth into the gas. We determine the dependence of the efficiency on the projectile energy in the present paper.

Some previous attempts have been made to obtain secondary electron distributions produced by cosmic ray sources,[10,11] however, they have been limited to high energy secondary electrons ($\gtrsim 100$ keV). The results we obtain here are intended to provide secondary electron distributions over a very large range of primary and secondary energies necessary for many applied purposes. These are the first results to our knowledge of detailed apportionment of an incident relativistic projectile's energy into various modes of excitation.

II. FORMULATION

A. Relativistic generalized oscillator strengths

The theoretical treatment of inelastic cross sections at relativistic energies was originally given by Bethe[12,13] and is valid so long as coupling to the radiation field can be neglected. This situation prevails over a large domain of incident energies, for electrons, for example, with kinetic energy, $E \lesssim 10^9$ eV.[14] The relativistic form for the differential scattering cross section is given by[12,13,14]

$$d\sigma_j/d\Omega = 4e^2\hbar^{-4}c^{-4}\epsilon\epsilon'(k'/k)\left|\eta_j(K)\right|^2 \times[K^2-(\epsilon-\epsilon')^2\hbar^{-2}c^{-2}]^{-2}\,. \quad (1)$$

Where e is the electronic charge, $\hbar$ is Planck's constant divided by 2π, c is the speed of light, ϵ and ϵ' are the total energy including the rest energy before and after the collision, respectively, k and k' are the incident and final wave numbers, K is the magnitude of the momentum transfer and $\eta_j(K)$ is the relativistic form factor for excitation of the state j. Central to our evaluation of Eq. (1) is an approximation due to Bethe[12,13] (cf. Ref. 14) which relates the nonrelativistic generalized oscillator strength to the square of the relativistic form factor, viz.,

$$\left|\eta_j(K)\right|^2 \simeq \begin{cases} QRf_j(K)/W_j, & (Ka_0 \gtrsim 1) \\ QRf_j(K)/W_j - W_j^3 f_j(0)(1-\beta^2)/(2mc^2R^2)\,, & (Ka_0 \ll 1) \end{cases} \quad (2)$$

where

$$Q = (Ka_0)^2 - (W_j^2/2mc^2R)$$

is a dimensionless form of the four momentum transfer, a_0 is the Bohr radius, R is the Rydberg energy, $f_j(K)$ is the nonrelativistic generalized oscillator strength, m is the electron rest mass, β is the ratio of the projectile velocity, v, to the speed of light, c, and W_j is the energy loss. This expression is valid for energy loss $W_j \ll mc^2 \approx 0.511$ MeV. This domain of validity is a serious restriction only when considering the production of high energy secondary electrons. However, as discussed later, in this limit the secondary electron may be regarded as free. Consequently, there are no serious difficulties in implementation which result from this restriction, at least for light atoms or molecules.

The total cross section for excitation of the jth discrete state can be shown to be

$$\sigma_j = \frac{2q_0}{mv^2R}\int_{x_l}^{x_u}\frac{|\eta_j(x)|^2\,dx}{(x - W_j^2/2mc^2R)^2}\,, \tag{3}$$

where $x=(Ka_0)^2$. x_l and x_u are the minimum and maximum momentum transfer values, which are determined from the conservation of energy and momentum, viz.,

$$\epsilon = (m_p^2c^4 + \hbar^2k^2c^2)^{1/2} = \epsilon' + W_j\,,$$

and

$$\mathbf{K} = (\mathbf{k} - \mathbf{k}')\,.$$

Here, $q_0 = 4\pi a_0^2R^2$ and has the numerical value 6.513×10^{-14} eV$^2\cdot$ cm^2, m_p is the rest mass of the projectile and the other symbols have their previous meanings. Clearly no distinction is made between incident projectiles except for charge and mass.

B. Allowed discrete excitations

Equation (3) for the total cross section coupled with Expression (2) gives rise to the following form for allowed discrete excitation, owing to the form of the generalized oscillator strengths[12,13]

$$\sigma_j = \frac{q_0 f_j(0)}{(m\beta^2c^2/2W_j)W_j^2}\left\{\ln\left[4\left(\frac{m\beta^2c^2}{2W_j}\right)\frac{C_j}{(1-\beta^2)}\right] - \beta^2\right\}. \tag{4}$$

Here $f_j(0)$ is the optical oscillator strength and C_j is a factor that is determined from the shape of the generalized oscillator strength. For most practical applications, C_j can be chosen as a constant independent of energy at high energy.

Clearly, however, this form of the cross section, while reducing to the nonrelativistic Bethe asymptotic cross section, is not applicable at low energies where the Born approximation breaks down. Consequently, we have made use of our previous work where the low energy behavior of the cross section was stressed,[4-9] viz.,

$$\sigma_j = \frac{q_0 f_j(0)\phi(2W_j/m\beta^2c^2)}{(m\beta^2c^2/2W_j)W_j^2}\left\{\ln\left[\frac{4(m\beta^2c^2/2W_j)C_j}{(1-\beta^2)} + e\right] - \beta^2\right\}, \tag{5}$$

where $\phi(2W_j/m\beta^2c^2)$ is a distortion factor and allows for variations from the asymptotic Bethe formula at low energy. Explicitly

$$\phi\left(\frac{2W_j}{m\beta^2c^2}\right) = \left[1 - \left(\frac{2W_j}{m\beta^2c^2}\right)^{\alpha_1}\right]^{\beta_1}\theta\left(\frac{m\beta^2c^2}{2W_j} - 1\right), \tag{6}$$

where

$$\theta\left(\frac{m\beta^2c^2}{2W_j} - 1\right) = \begin{cases} 1, & (m\beta^2c^2/2) \geq W_j \\ 0, & (m\beta^2c^2/2) < W_j\,. \end{cases}$$

The factor e in Eq. (5) allows C_j to be chosen a constant equal to the asymptotic value in Eq. (4) while the parameters of Eq. (6) are used to determine the low energy behavior. Based upon previous generalized oscillator strength and cross section assignments,[6-9] we have determined the optical oscillator strength, and the parameters C_j, α_1, β_1 appearing in Eq. (5) and tabulated in Table I. (It has been found convenient in previous work to also treat W_j as a parameter to fit some states close to threshold.)

TABLE I. Cross section parameters for electron and proton impact.

		Electron					Proton	
Allowed states		W_j(eV)	$f_j(0)$	C_j	α_1	β_1	J	v
N_2								
$b\,^1\pi_u$		12.5	0.666	0.056	1.24	3.66	1.98	1.0
$b'\,^1\Sigma_u^+$		13.3	0.321	0.061	1.29	3.72	1.83	1.0
O_2								
$B\,^3\Sigma_u^-$		8.4	0.254	0.037	1.19	2.31	3.35	0.5
9.9 eV peak		9.9	0.0285	0.622	1.38	3.44	4.44	0.5
N_2 Rydbergs								
Quantum defect ρ			F^*					
0.7	$X\,^2\Sigma_g^+$	15.58	5.11	0.062	1.18	3.44	1.8	1.0
1.04	$A\,^2\pi_u$	16.73	2.24	0.065	1.17	3.42	1.8	1.0
0.87	$B\,^2\Sigma_u^+$	18.75	1.16	0.075	1.16	3.36	1.8	1.0
1.53	$D\,^2\pi_g$	22.0	0.784	0.082	1.15	3.32	1.8	1.0
0.8	$C\,^2\Sigma_u^+$	23.6	0.784	0.096	1.13	3.25	1.8	1.0
0.8	40 eV state	40.0	1.12	0.096	1.13	3.25	1.8	1.0
O_2 Rydbergs								
Quantum defect ρ			F^*					
1.08	$X\,^2\pi_g$	12.1	0.688	0.044	1.22	3.71	2.40	0.8
1.00	$a\,^1\pi_u$	16.1	1.634	0.062	1.18	3.44	2.40	0.8
1.07	$A\,^2\pi_u$	16.9	1.634	0.065	1.17	3.41	2.40	0.8
0.69	$b\,^1\Sigma_g^+$	18.2	1.462	0.073	1.16	3.36	2.40	0.8
1.00	$B\,^2\Sigma_g^-$	20.3	0.946	0.093	1.14	3.28	2.21	0.8
1.00	$c\,^1\Sigma_u^-, ^2\pi$(III)	23.0	1.376	0.093	1.14	3.28	2.21	0.8
1.00	37 eV	37.0	0.86	0.093	1.14	3.28	2.21	0.8
Forbidden states		W_j(eV)	F_j	Ω	α_1	β_1	J	v
N_2								
vib v 1 – 3		1.85	0.273	7.0	1.0	1.0	1.32	2.0
vib v 4 – 8		2.15	0.241	9.0	1.0	1.0	1.28	2.0
$A\,^3\Sigma_u^+(VK)$		8.00	0.226	3.0	1.0	1.0		
$B\,^3\pi_g$ (first pos.)		8.50	0.178	3.0	3.0	1.0		
$C\,^3\pi_u$ (second pos.)		11.05	0.28	3.0	3.0	1.0		
$E\,^3\Sigma_g^+$		11.9	0.048	3.0	3.0	1.0		
$a\,^1\pi_g$ (LBH)		8.6	0.136	1.0	1.0	1.0	0.994	1.0
$a''\,^1\Sigma_g^+$		12.25	0.027	1.0	2.3	1.0	0.667	2.0
O_2								
$b\,^1\Sigma_g^+$		1.64	0.0005	3.0	3.0	1.0		
$a\,^1\Delta_g$		0.98	0.0005	3.0	3.0	1.0		
$A\,^3\Sigma_u^+$		4.5	0.021	0.9	1.0	1.0	2.13	0.5

Rydberg series are treated as in our previous work. Here, the magnitude of the optical oscillator strength is assumed to vary as

$$f_n(0) = F^*/(n-\rho)^3\,,$$

where F^* is a constant for the Rydberg series in question, n is the principle quantum number, and ρ is the quantum defect for the series. The C_n appearing in Eqs. (4) and (5) is also assumed to be independent of n for $n \geq n_i$, where n_i is conveniently chosen equal to 5 for the present determinations. Consequently, we may sum the contribution to all higher lying members.

$$\sigma_{n\geq n_i} \simeq \frac{q_0 F^* \phi(2W_R/m\beta^2c^2)}{2(n_i-\rho-\frac{1}{2})^2(m\beta^2c^2/2W_R)} \times\left\{\ln\left[\frac{4(m\beta^2c^2/2W_R)C_{n_i}}{(1-\beta^2)}+e\right]-\beta^2\right\} \quad (7)$$

where

$$W_R \equiv I - R/(n_i-\rho)^2 .$$

Tabulations of these parameters for the important states of N_2 and O_2 are also shown in Table I.

Equation (4) may also be shown to hold for proton excitation of discrete allowed states, where β is determined appropriately for protons. We neglect, here, motion of the center of momentum frame. At low energy where breakdown of the Born approximation is evident, the proton cross sections are found to have shapes different than those obtained for electrons. Consequently, we make use of our previous work on proton cross sections[15-18] to obtain an analytic form which behaves as Eq. (4) in the high energy domain but at low energy like our previous determinations. Here, we define $\phi(2W_j/m\beta^2c^2)$ appearing in Eq. (5) for protons by

$$\phi\left(\frac{2W_j}{m\beta^2c^2}\right)=\frac{(m\beta^2c^2/2W_j)^{\nu+1}}{J^{\nu+1}+(m\beta^2c^2/2W_j)^{\nu+1}} . \quad (8)$$

The parameters J and ν for the proton cross sections are given in Table I. Proton excitation of Rydberg series is treated as in Eq. (7) with $\phi(2W_j/m\beta^2c^2)$ given by Eq. (8). We have taken 1 GeV, as a practical upper energy limit for protons since no nuclear cross sections are presently considered.

C. Forbidden excitations

Optically forbidden transitions for which $f_j(0)=0$ are evaluated in an analogous manner from Eq. (2) and Eq. (3), viz.,

$$\sigma_j=\frac{q_0 F_j}{(m\beta^2c^2/2W_j)W_j^2} ,$$

where

$$F_j=\int_{x_i}^{x_u}\frac{|\eta_j(x)|^2}{(x-W_j^2/2mc^2R)^2}\,dx . \quad (9)$$

For applied purposes, these cross sections are important only at low energies. Borrowing again upon our previous work,[4-9] we have used the form

$$\sigma_j=\frac{q_0 F_j \phi(2W_j/m\beta^2c^2)}{(m\beta^2c^2/2W_j)W_j^2} , \quad (10)$$

where

$$\phi\left(\frac{2W_j}{m\beta^2c^2}\right)=\frac{[1-(2W_j/m\beta^2c^2)^{\alpha_1}]^{\beta_1}}{(m\beta^2c^2/2W_j)^{\Omega-1}} ,$$

to span the full energy range. The parameters F_j, α_1, β_1, Ω are determined in accord with our previous cross section determinations at *low energies*. Eq. (9) also describes the asymptotic proton cross section. The proton low energy distortion parameter ϕ is chosen as

$$\phi\left(\frac{2W_j}{m\beta^2c^2}\right)=\frac{(m\beta^2c^2/2W_j)^{\nu+1}}{J^{\Omega+\nu}+(m\beta^2c^2/2W_j)^{\Omega+\nu}} . \quad (11)$$

Proton excitation of N_2 and O_2 involving a change of multiplicity is treated as being strictly forbidden, $F_j=0$. The parameters J and ν are listed in Table I.

D. Continuous processes

The approximation of Eq. (2) for the relativistic form factor may be generalized for continuous processes (for $W \ll mc^2$) to

$$|\eta(K,W)|^2=\begin{cases} Q\dfrac{R}{W}\dfrac{df(K,W)}{dW} & (Ka_0 \gtrsim 1) \\ Q\dfrac{R}{W}\dfrac{df(K,W)}{dW}-\dfrac{W^3(1-\beta^2)}{R^2 2mc^2}\dfrac{df(0,W)}{dW} , & (Ka_0 \ll 1) \end{cases} \quad (12)$$

where $\eta(K,W)$ is the relativistic form factor for excitation of the continuum per unit range of energy loss W, $[df(K,W)/dW]$ is the nonrelativistic generalized oscillator strength density per unit range of energy loss W, and the other symbols are as defined previously. The cross section for production of secondary electrons per unit range of energy loss W, for incident kinetic energy, E, denoted by $S(E,W)$, is then given by

$$S(E,W)=\frac{q_0}{(m\beta^2c^2/2)W}\int_{x_i}^{x_u}\frac{|\eta(K,W)|^2\,dx}{[x-(W^2/2mc^2R)]^2} . \quad (13)$$

To obtain relativistic determinations of $S(E,W)$, we have made use of an analytic parametrization of the Massey–Mohr–Bethe surface of hydrogen,[19] viz.,

$$\frac{df(x,w)}{d(W/R)}=\frac{A\gamma^3[x+\frac{1}{3}w]\,w\exp[-(2/\alpha_2)\arctan\alpha_2]}{[(x-\beta_1 w)^2+4\gamma x]^3[1-\exp(-2\pi/\alpha_2)]} , \quad (14)$$

where $w=W/I$ is a reduced energy loss, $\alpha_2=[w-1]^{1/2}$, I is the ionization potential and A, γ, and β_2 are parameters which are considered to be functions of W. While this form appears rather restricted and will not fit the complex shapes for some atoms (cf. Ref. 20), we have found it to be surprisingly versatile in representing a variety of Bethe surfaces. It has proven to be quite successful in representing the Bethe surface calculated for neon[20] and atomic oxygen[21] as well as the restricted range of the Bethe surface for N_2 and O_2 empirically determined by Silverman and Lassettre.[22,23]

This form has a number of useful features. For example, it can be simply integrated when substituted into Eq. (13). In addition, it behaves correctly for large values of the energy loss by picking up the Bethe ridge. This latter behavior is important both for establishing the W^{-2} behavior at large energy loss and for satisfying the Bethe sum rule. The use of this form is restricted by Eq. (12) for $W \ll mc^2$, which we have interpreted practically as $W \simeq 10^4$ eV for the present considerations. As has been mentioned previously, at such large values of energy transfer the secondary electron can be treated as free. The values of $S(E,W)$ for $W > 10^4$ eV can be obtained directly from the Moller cross section.[24] The exchange corrections in the Moller cross section must be set to zero for proton initiated ionizations. The large energy transfer region for proton impact will be treated using a modification of the Bhabha cross section.[25]

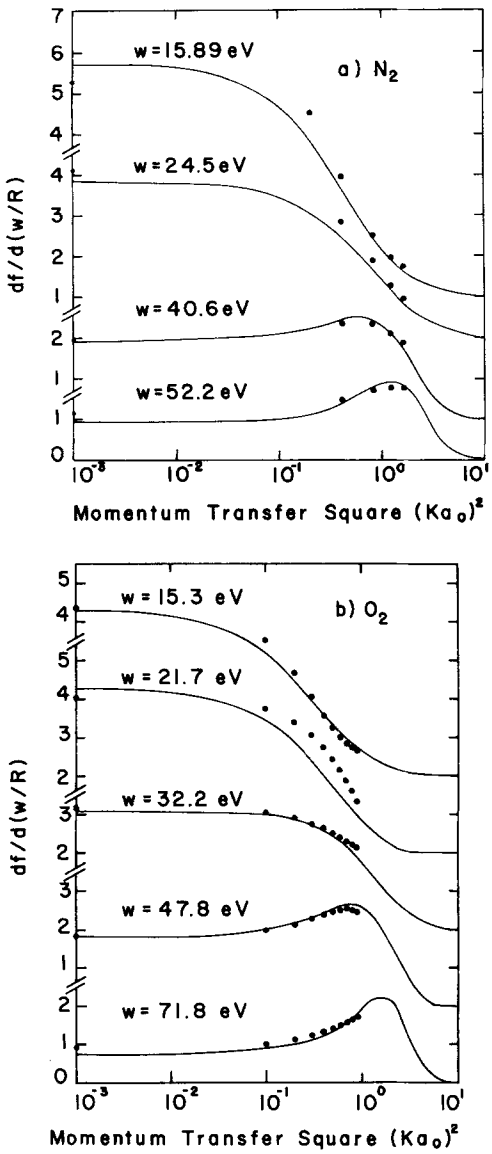

FIG. 1. Comparison of empirically determined[22,23] $df/d(w/R)$ with Eq. (14) (see text). (a) N_2 and (b) O_2.

To obtain the parameters appearing in Eq. (14) we have simultaneously fit (1) the available empirical continuum generalized oscillator strength data[22,23]; (2) the differential cross section data[26,27] for secondary electron ejection; (3) the Bethe sum rule; and (4) the total ionization cross section data.[28] For simplicity in obtaining relativistic $S(E, W)$ values we have assumed that the shape of each ionization continuum making up the total Bethe surface for each respective gas is constant. The ionization potential I has, consequently, been treated as an "effective" ionization potential in fitting the manifold of ionization continua making up each gas. The fraction of the total Bethe surface contributed by each continua is given by A_c/A where $A=\sum_c A_c$ and c runs over the number of continua. For consistency we have set

$$F_c^* = 27.2\,\frac{A_c}{A}\,\frac{df}{dW}(0,W)\Big|_{W=I},$$

where F_c^* is the Rydberg optical oscillator strength constant for continua c. These assignments are made compatible with the branching ratio determinations to be discussed later as well as with our previous assignments.[6-9]

In Fig. 1 we show a comparison of the Bethe surface calculated from Eq. (14) and the parameters of Table II with empirical determinations of Silverman and Lassettre.[22,23] As can be seen, the agreement is generally within 15%. In Fig. 2 we show a comparison of the $S(E, T)$ values (where $W=T+I$), as determined from Eq. (13) and the parameters of Table II, with the empirical determinations of Opal *et al.*[26] as normalized by Green and Sawada.[27] As can be seen the agreement here is again within about 15%. Either the $S(E, T)$ or the generalized oscillator strength data can be fit to substantially higher accuracy; however, the simultaneous fitting can be carried out at best to about 15%. We note that for the parametrizations given in Table II, the Bethe sum rule is satisfied to 10% or better out to $(Ka_0)^2$ values of 500. This range of $(Ka_0)^2$ covers the range of energy loss out to about 10^4 eV or the range of validity of Eq. (12).

E. Analytic parametrization of $S(E,T)$

While the functional form of Eq. (14) is analytically integrable over x, it can not subsequently be integrated analytically over W to arrive at the total cross section.

TABLE II. Bethe surface parameters.[a]

$$A=A_1\{(W-I+0.1)^{a_3}[(W-I)^{a_2}+a_1^{a_2}]^{-1}+a_4[a_5^{a_6}+(W-I)^{a_6}]^{-1}\}$$
$$\beta_2=b_1(W-I+0.1)^{b_4}[(W-I)^{b_3}+b_2^{b_3}]^{-1}$$
$$\gamma=g_1(W-I+0.1)^{g_4}[(W-I)^{g_3}+g_2^{g_3}]^{-1}$$

Parameter	N_2	Parameter	O_2
I	15.6 eV	I	15.2 eV
a_1	26.42 eV	a_1	1.389×10^3 eV
a_2	1.313	a_2	3.808×10^{-1}
a_3	1.608×10^{-3}	a_3	3.0×10^{-2}
a_4	9.70×10^{-7}	a_4	5.083×10^{-7}
a_5	1.826×10^2 eV	a_5	2.589×10^2 eV
a_6	−1.795	a_6	−2.097
b_1	1.137×10^3	b_1	6.557×10^2
b_2	6.088 eV	b_2	5.324 eV
b_3	2.448	b_3	2.269
b_4	1.081×10^{-2}	b_4	-1.411×10^{-4}
g_1	2.629×10^4	g_1	2.0×10^4
g_2	5.436 eV	g_2	5.287 eV
g_3	3.333	g_3	3.132
g_4	8.4×10^{-3}	g_4	-6.750×10^{-2}
$A_1(15.58)$[b]	1.567×10^4	$A_1(12.1)$	3.881×10^2
$A_2(16.73)$	6.868×10^3	$A_2(16.1)$	9.217×10^2
$A_3(18.75)$	3.571×10^3	$A_3(16.9)$	9.217×10^2
$A_4(22.0)$	2.404×10^3	$A_4(18.2)$	8.247×10^2
$A_5(23.6)$	2.403×10^3	$A_5(20.3)$	5.334×10^2
$A_6(40.0)$	3.434×10^3	$A_6(23.0)$	7.762×10^2
		$A_7(37.0)$	4.851×10^2
A_{total}	3.434×10^4	A_{total}	4.851×10^3

[a]With reference to Eq. (14).
[b]Values in parenthesis are the threshold energy.

It is convenient, for applied purposes, to obtain an expression which can approximate the results of Eq. (13) at high energies and the empirical $S(E, T)$ data at low energies, thus covering the *full* energy range from near threshold to ~ 100 MeV electron energy but yet possesses an analytic form when integrated over W. Green and Sawada[27] have used an analytic form similar to the Breit–Wigner form used in nuclear physics to parametrize the Opal *et al.*[26] $S(E, T)$ data. We have modified this functional form to have the correct relativistic behavior of Eq. (4) for the total ionization cross section. This behavior essentially results from the small energy loss behavior $W \lesssim 500$ eV. A further modification of the Breit–Wigner form has been incorporated to include exchange and spin dependent corrections at high energy and energy loss values, viz.,

$$S(E,T)=\sum_j \frac{F_j(E)}{(m\beta^2c^2/2)}\left(K\Gamma^2(E)\left\{\ln\left[4\left(\frac{m\beta^2c^2}{2I_j}\right)\frac{C_j}{(1-\beta^2)}\right]-\beta^2\right\}\left(\frac{1}{(T-T_0)^2+\Gamma^2(E)}-\frac{B(E)}{(T-T_1)^2+\Gamma_1^2}\right)\right.$$
$$\left.+N_e\pi e^4\left(\frac{1}{(E-T-I_j)^2+\Gamma_2^2}+\frac{1}{(E+mc^2)^2}-\frac{2Emc^2+(mc^2)^2}{(E+mc^2)^2}\,\frac{1}{(T+I_j)(E-T-I_j)+\Gamma_2^2}\right)\right), \tag{15}$$

where N_e is the number of electrons of the neutral molecular species. $F_j(E)$ is an energy dependent amplitude factor for the ionization continuum j and j runs over the number of continua. The last term of this expression on the top line embodies the Breit–Wigner form of Green and Sawada[27] at low energy and the behavior of Eq. (13) at high energy. The factor $B(E)$ reduces the magnitude of the relativistic rise of Eq. (4) to match with the magnitude of the $(m\beta^2c^2/2)^{-1}W^{-2}$ behavior in the Moller cross section at high energy loss values. The remaining terms are just the Moller corrections for spin and exchange. The factor Γ_2 is introduced to cancel these terms at incident energies below about 1 keV.

The parameters appearing in Table III have been obtained by fitting the shape of the low energy empirical data of Opal *et al.*[26] and then normalizing to the total ionization cross section of Rapp and Golden.[28] The high energy behavior is fit to the results obtained from Eq. (13) which join smoothly to the Moller cross section at large energy loss.

A comparison of the N_2 total ionization cross section obtained from Eq. (15) and the parameters of Table III is shown in Fig. 3 with empirical determinations.[28,29] A comparison of $S(E, T)$ computed from Eq. (15) and the parameters of Table III is shown in Fig. 4 with results of Opal *et al.*[26] and Green and Sawada[27] and the high energy results computed from Eq. (13) using the parameters of Table II. In general the agreement is better that 15% over the full primary and secondary energy domain. Some differences larger than 15% occur, however, usually at small values of the secondary energy ($T \lesssim 7$ eV) where the empirical results are of greatest uncertainty. In view of this general agreement and the range of experimental uncertainties, there appears to be no serious disadvantage to the use of Eq. (15) for most applied purposes. Similar accuracy is obtained for O_2 using the parameters of Table III.

In the treatment of secondary electron production by proton bombardment we make use of the work of Bhabha[25] at large energy transfer which we have modified slightly for use at low incident kinetic energies as well.

$$S(E,T)=\sum_j \frac{F_j(E)}{(m\beta^2c^2/2)}\left\{K\Gamma^2(E)\left[\ln\left(\frac{4m\beta^2c^2C_j}{2I_j(1-\beta^2)}+e\right)-\beta^2\right]\right.$$
$$\left.\cdot\left(\frac{1}{(T-T_0)^2+\Gamma^2(E)}-\frac{B(E_e)}{(T-T_1)^2+\Gamma_1^2}\right)+N_e\pi e^4\left[(2(E+2m_pc^2))^{-2}-(T_m+I_j+\delta)^{-1}(T+I_j)^{-1}\right]\right\}, \tag{16}$$

where N_e is the number of electrons of the neutral molecule; $F_j(E)$ is a low energy amplitude distortion factor for the continuum j, and m_p is the projectile rest mass. The factor $B(E_e)$ in the second bracket has as its argument the electron kinetic energy corresponding to an electron moving with the projectile velocity. The purpose of this term is again to reduce the magnitude of the relativistic rise to the $(\frac{1}{2}m\beta^2c^2)^{-1}W^{-2}$ behavior expected in the Bhabha cross section[25] for larger values of W. The last term in brackets describes the deviations from this behavior at large energy transfer and reduces to the Bhabha[25] form at high incident energy. The parameter δ has been inserted to prevent domination by this term at small values of the proton kinetic energy. T_m appearing here is the maximum energy transfer to a free stationary electron and is given by[25]

$$T_m=\frac{E(E+2m_pc^2)}{(E+mc^2)+(m_p/m)(E+m_pc^2)},$$

where E is the projectile kinetic energy. It is assumed that the proton has a point magnetic moment equal in magnitude to that of an electron. At the cutoff energies for protons presently considered, there is no error introduced by this approximation. If extrapolation to considerably higher energy is desired, form factors for the charge and anomalous magnetic moment must be considered.[30]

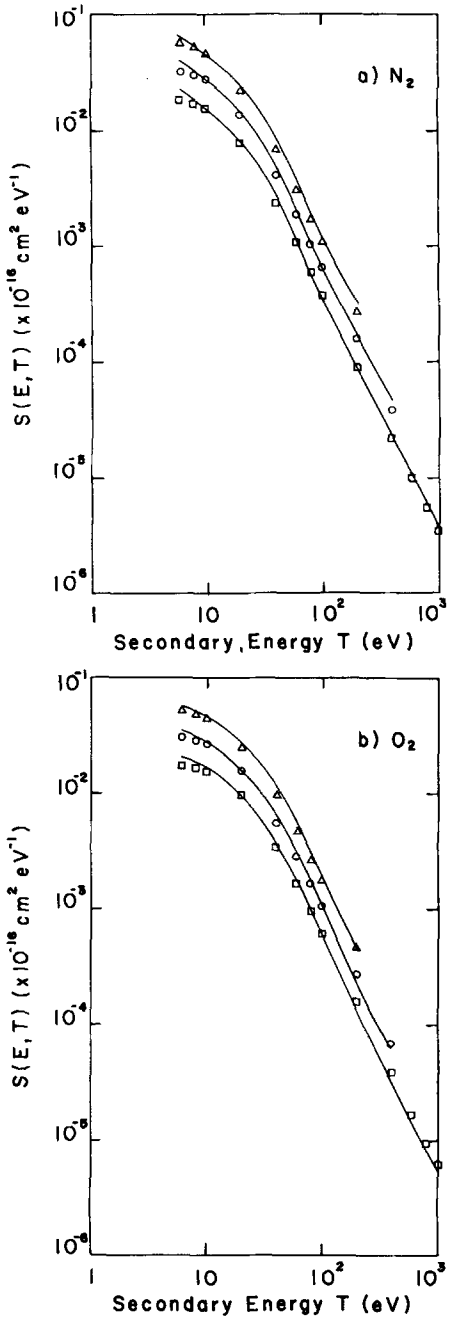

FIG. 2. Comparison of empirically fit $S(E,T)$[27] with results of Eq. (14). (see text). (a) N_2 and (b) O_2.

TABLE III. $S(E,T)$ parameters for electron and proton impact.

Electrons[a]

$$F_j(E) = f_j\left(\frac{D_j}{D_j - \exp[-(E-I_j)/\alpha I_j]}\right) \qquad B(E) = B_0\,[\ln(E/E_0)^2 + B_1]$$

$$\Gamma(E) = \Gamma_s + \frac{\Gamma_0\Gamma_B^2 E}{[(E-E_\Gamma)^2+\Gamma_B^2]} \qquad \Gamma_2(E) = \left[\frac{A_1 E}{E-I_j}\right]$$

$$T_0(E) = T_s - \frac{T_A}{(E+T_B)}$$

Parameter	N_2	O_2	Parameter	N_2	O_2
B_0	0.029	0.030	K	7.58×10^{-16}	6.55×10^{-16}
B_1	1.035	1.035	Γ_s (eV)	11.1	13.1
E_0(eV)	8239	8239	Γ_0	0.029	3.06
T_1	53.3	68.3	Γ_B(eV)	51.3	25.6
Γ_1	115	189.1	E_Γ (eV)	61.5	129.1
N_e	14	16	T_s	4.0	6.34
A_1(eV)	5000	5000	T_A	2450	4101
α	2.3	7.64	T_B	63.8	78.4

	j	I_j	f_j	D_j	C_j
N_2	1	15.58	0.456	4.23	2.48
	2	16.73	0.2	2.3	2.66
	3	18.75	0.104	3.35	2.99
	4	22.	0.07	200	3.50
	5	23.6	0.07	200	3.76
	6	40	0.1	200	6.37
		...	...	...	...
O_2	1	12.1	0.08	1.16	1.93
	2	16.1	0.19	1.57	2.56
	3	16.9	0.19	200	2.69
	4	18.2	0.17	200	2.90
	5	20.3	0.11	200	3.23
	6	23	0.16	200	3.66
	7	37	0.1	200	5.89

Protons[b]

Parameters K, T_S, Γ_S, T_1, Γ_1, C_j, f_j, and the function $B(E_e)$ are the same as above

$$\Gamma(E) = \frac{\gamma_1}{(\frac{1}{2}m\beta^2c^2+\gamma_2)} + \Gamma_S$$

$$T_0(E) = T_S - \frac{t_a}{(\frac{1}{2}m\beta^2c^2+t_b)}$$

$$F_j(E) = \frac{(\frac{1}{2}m\beta^2c^2)^{\nu+1}f_j}{(J)^{\nu+1}+(\frac{1}{2}m\beta^2c^2)^{\nu+1}}\ .$$

Parameter	N_2	O_2
γ_1 (eV)	1.27×10^4	5.0×10^5
γ_2 (eV)	1.81×10^3	7.60×10^4
t_a (eV)	2.03×10^4	2.52×10^3
t_b (eV)	1.97×10^3	1.28×10^2
J (eV)	3.39	40.3
ν	-1.93×10^{-1}	3.14×10^{-1}
δ (eV)	84.0	132.1

[a]With reference to Eq. (15). [b]With reference to Eq. (16).

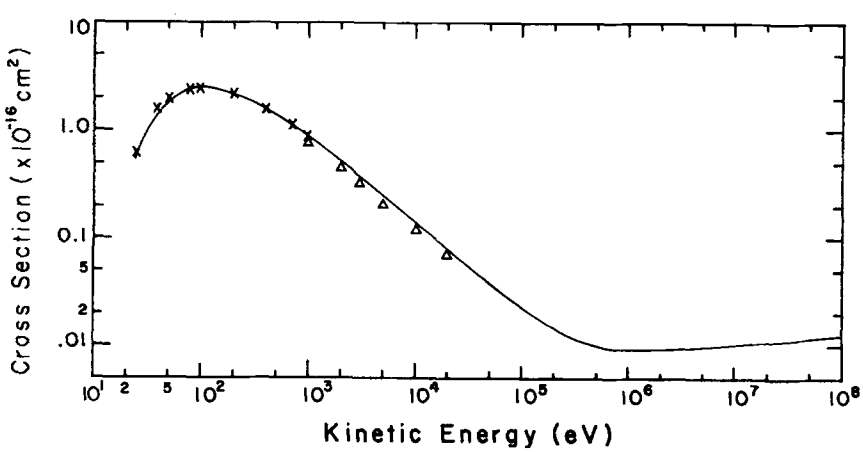

FIG. 3. Comparison of the calculated N_2 ionization cross section from Eq. (15) with the empirical determinations of Rapp and Golden[28] and Schram *et al.*[29] (Δ).

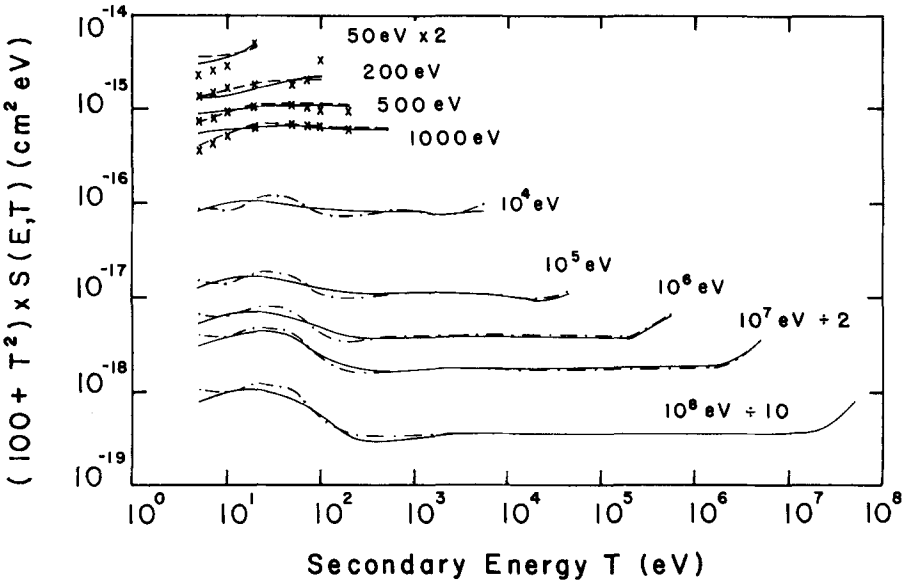

FIG. 4. Comparison of the calculated electron N_2 $S(E, T)$ cross section from Eq. (15) (—) with Opal *et al.*[26] (x), Green and Sawada[27] (- - -), and the high energy results from Eq. (13) and the Moller cross section (•--•).

A comparison of the results of Eq. (16) using the parameters of Table III and the empirical $S(E, T)$ data of Crooks and Rudd[31] and Toburen[32] is shown in Fig. 5. A comparison of the total ionization cross section computed from Eq. (16) and various empirical determinations is shown in Fig. 6. Clearly the agreement is acceptable for most applied purposes. A similar accuracy is obtained for O_2 and the parameters of Table III. For completeness we note that the empirical data[31,32] indicates that secondary electrons may be produced at energies above the classical impact cutoff T_m. Owing to the very rapid drop off in the probability for production of these electrons, however, we have chosen T_m as a practical cutoff.

We have made no attempt to separate out the K shell ionization processes in our analysis. A previous discussion by Khare[33] indicates that the K shell ionization cross section is about 1% of the total ionization cross section in N_2. A similar percentage would also be expected for O_2. Some alteration in the shape of $S(E, T)$ is expected due to Auger electrons. However, a recent calculation by Soong[34] shows that Auger electrons in neon produced by 10^5 eV primary electrons contribute only about 3% to the degradation spectrum. In view of the empirical uncertainties ~ 10%, we have not attempted at this time to incorporate the Auger spectrum into our $S(E, T)$ results.

III. BRANCHING RATIOS FOR DISSOCIATION

A. Nitrogen

Molecular nitrogen is a very stable homonuclear molecule in which both singlet and triplet states are found to be strongly bound. As a consequence, dissociation of the molecule via the direct excitation of repulsive states is almost nonexistent. On the other hand, measurements of the total dissociation cross section by Winters[35] and the dissociative ionization cross section by Rapp *et al.*[36] indicate that processes leading to dissociation of the N_2 molecule are highly probable. The main processes appear to be predissociation of stable electronic terms by repulsive states that are themselves strongly optically forbidden in direct excitation. As a consequence of this, dissociation processes in N_2 are not "new" processes to be included in competition with other excitation processes when considering energy apportionment, but rather are final products that result from given excitations.

We define the branching ratio for predissociation (i.e., the fraction of excitations of the vibrational level ν' of the electronic term k that predissociate) by

$$B_{\nu',k}=\frac{I_{\nu',k}}{A_{\nu',k}+I_{\nu',k}+AI_{\nu',k}+S_{\nu',k}},$$

where $I_{\nu',k}$ is the rate for spontaneous predissociation, $A_{\nu',k}$ is the total rate for spontaneous radiative transi-

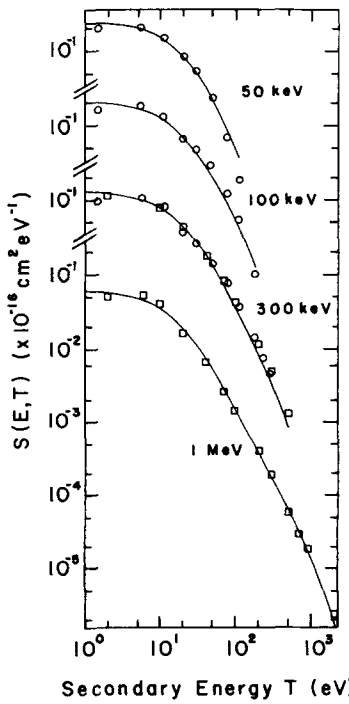

FIG. 5. Comparison of the calculated proton N_2 $S(E, T)$ cross section from Eq. (16) (—) with the empirical data of Rudd[31] (o) and Toburen[32] (□) at various incident energies.

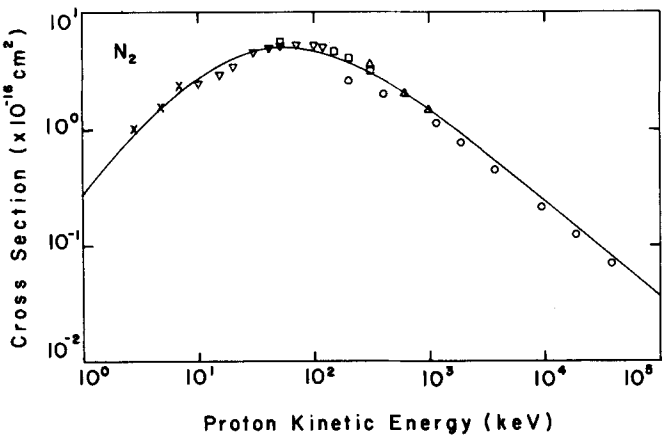

FIG. 6. Comparison of the calculated total proton ionization cross section determined by integration of Eq. (16) with various empirical determinations. Protons: McNeal and Clark[62] (x); deHeer *et al.*[63] (▽); Hooper (△); Crooks and Rudd[31] (□). Electrons: Shhram *et al.*[29] (○).

tion, $AI_{\nu',k}$ is the rate for spontaneous autoionization and $S_{\nu',k}$ is the quenching rate for the vibrational level ν' of the electronic state k. It is clear from this expression that a knowledge of each of these rate coefficients is required if the branching ratio for predissociation is to be determined. Unfortunately, at the present, only fairly rough estimates of the various rates can be obtained from the literature.

Our analysis for the $a\,^1\pi_g$, $C\,^3\pi_u$ and $b\,^1\pi_u$ states in N_2 follows closely that given by Polak *et al.*[37] Predissociation of the $a\,^1\pi_g$ state of N_2 is observed for $\nu' \geq 6$.[38,39] This predissociation is heterogeneous and thought to occur via the $^5\Sigma_g^+$ state. Consequently it is dependent on the rotational temperature. Polak *et al.*[37] estimate

$$I_{\nu'\geq 6,a\,^1\pi_g} \simeq 1.4\times 10^3 T_j \text{ sec}^{-1} ,$$

where T_j is the rotational temperature. The radiative transition rate is about[40]

$$A_{\nu',a\,^1\pi_g} \simeq 7.1\times 10^3 \text{ sec}^{-1} .$$

We will neglect the quenching of the $a\,^1\pi_g$ state and other states for the present purposes of obtaining an effective dissociation cross section to compare with empirical measurements. Assuming a rotational temperature of 300 °K and folding in these rate estimates with the Franck–Condon factors of Nicholls[41] we obtain the net branching ratio for predissociation from the $a\,^1\pi_g$ state shown in Table IV. We also show here the expected dissociation products.

The $C\,^3\pi_u$ state is observed to have two different types of predissociation.[42] One of these occurs via the $^5\pi_u$ interaction and the other via the $C'\,^3\pi_u$ interaction. Polak *et al.*[37] estimate that, for the important levels

$$A_{\nu',C\,^3\pi_g} \approx 2\times 10^7 \text{ sec}^{-1} ,$$

while

$$I_{\nu',C\,^3\pi_g} \approx 1\times 10^8 \text{ sec}^{-1} .$$

Folding these estimates into the Franck–Condon factors of Zare *et al.*[43] we arrive at the net predissociation branching ratio for the $C\,^3\pi_g$ state shown in Table IV. The dissociation fragments assumed are also shown here.

Many vibrational levels of the $b\,^1\pi_u$ state of N_2 are observed to be diffuse in absorption and absent in emission[44] probably indicating predissociation. The predissociation apparently occurs via the $C'\,^3\pi_u$ state[44] and consequently is homogeneous and does not depend upon the rotational temperature. We have used the $I_{\nu',b\,^1\pi_u}$ estimates of Polak *et al.*[37] based upon absorption widths and an estimate of 1.5×10^9 sec^{-1} for $A_{\nu',b\,^1\pi_u}$. Folding these rates into the Franck–Condon factors of Nicholls[41] we arrive at the net branching ratio for predissociation shown in Table IV. The dissociation fragments are assumed to be $N(^4S^0)$ and $N(^2D^0)$, consistent with predissociation via the $C'\,^3\pi_u$ state. Only brief discussions of the $b'\,^1\Sigma_u^+$ are presented in the literature, however, higher vibrational levels are absent in emission and breaking off of the rotational structure in emission[45,46] indicates predissociation. In the absence of more detailed accounts, we have assumed that the branching ratio for predissociation of the $b'\,^1\Sigma_u^+$ state is equal to that of the $b\,^1\pi_u$ state. The predissociation is assumed to occur via a $^3\Sigma_g^+$ state giving the fragments shown in Table IV.

The Rydberg series in N_2 that converge to the N_2^+ $X\,^2\Sigma_g^+$ state as well as the members of other Rydberg series that lie below the lowest ionization threshold cannot autoionize. However, there is evidence for strong predissociation here[44,45] and Zipf[47] has suggested that the Rydberg states of $^1\pi_u$ symmetry are predissociated by the $C'\,^3\pi_u$ state. Since these levels are optically allowed and are not observed in emission, they must have predissociation rates comparable to the $I_{\nu',b\,^1\pi_u}$. In the absence of a more detailed understanding, we have set $I_{\nu',R} \gtrsim 10A_{\nu',R}$ for those Rydberg levels with thresholds less than the lowest ionization threshold. The dissociation fragments for each of these levels are assumed to be $N(^4S^0)+N(^2D^0)$.

Cook and Ogawa[48] have determined photoionization branching ratios for some Rydberg levels lying above the lowest ionization threshold. Since these states are not observed strongly in emission and have autoionization branching ratios of roughly about 0.5, the rates satisfy $I_{\nu',R} \simeq AI_{\nu',R}$ for small n values $n \leq 5$. Assuming a rough n dependence of n^{-3} for the autoionization rates as discussed by Freund,[49] we determined the branching ratios for predissociation summed for $n \geq 5$ as shown in Table IV. The assignment of dissociation fragments for these high-lying Rydbergs is somewhat arbitrary. However, owing to the considerable effort in determining cross sections for N I emissions[50a–50c] resulting from electron impact on N_2, we have some idea of the higher levels of excitation of the dissociation fragments. The assignments shown in Table IV give good agreement with the cross sections as determined above. The dissociation fragments for the remaining Rydberg levels lying above the ionization threshold have been arbitrarily assigned by choosing an appearance potential close to but below the Rydberg level threshold.

The processes leading to dissociative ionization in N_2 are only poorly understood.[51,52] There appear to be

TABLE IV. Branching ratios for predissociation and dissociation.

N_2 Excited state	Branching ratio	Dissociation products
$a\,^1\pi_g$(LBH)	0.2	$N(^4S^0) + N(^4S^0)$
$b\,^1\pi_u$	0.8	$N(^4S^0) + N(^2D^0)$
$b'\,^1\Sigma_u^+$	0.8	$N(^4S^0) + N(^2D^0)$
$C\,^3\pi_u$(sec. pos.)	0.5	$N(^4S^0) + N(^4S^0)$

Rydberg

Principle quantum number	Branching ratio	Dissociation products	Principle quantum number	Branching ratio	Dissociation products
	$X\,^2\Sigma_g^+$			$A\,^2\pi_u$	
$n=3$	1.0	$N(^4S^0) + N(^2D^0)$	$n=3$	1.0	$N(^4S^0) + N(^2D^0)$
$n=4$	1.0	$N(^4S^0) + N(^2D^0)$	$n=4$	1.0	$N(^4S^0) + N(^2P^0)$
$n\geq 5$	1.0	$N(^4S^0) + N(^2P^0)$	$n\geq 5$	0.68	$N(^2D^0) + N(^2D^0)$
	$B\,^2\Sigma_u^+$			$D\,^2\pi_g$	
$n=3$	1.0	$N(^2D^0) + N(^2P^0)$	$n=3$	1.0	$N(^2D^0) + N(^2P^0)$
$n=4$	0.5	$N(^2D^0) + N(^2P^0)$	$n=4$	0.5	$N(^4S^0) + N(3s\,^2P)1493$
$n\geq 5$	0.68	$N(^2D^0) + N(^2P^0)$	$n\geq 5$	0.68	$N(^4S^0) + N(3s^4P)1200$
	$C\,^2\Sigma_u^+$			40 eV	
$n=3$	0.5	$N(^4S^0) + N(3s^2P)1493$	$n=3$	0.5	$N(^4S^0) + N(3s^2D)1243$
$n=4$	0.5	$N(^4S^0) + N(3s^4P)1200$	$n=4$	0.5	$N(^4S^0) + N(3s^2P)1743$
$n\geq 5$	0.68	$N(^4S^0) + N(3s^4P)1200$	$n\geq 5$	0.68	$N(^4S^0) + N(4s^2P)1177$

Ionization continua	Branching ratio	Dissociation products
$D\,^2\Pi_g$	1.0	$N(^4S^0) + N^+(^3P)$
$C\,^2\Sigma_u^+$	1.0	$N(^2D^0) + N^+(^3P)$

40 eV

Branching ratio	Dissociation products	Branching ratio	Dissociation products
0.228	$N^+(^3P) + N(3s^4P)1200$	0.019	$N(^4S^0) + N^+(^3P)916$
0.139	$N^+(^3P) + N(3s^2P)1493$	0.005	$N(^4S^0) + N^+(^1D)776$
0.077	$N^+(^3P) + N(3s^2P)1743$	0.007	$N(^4S^0) + N^+(3s\,^1P)746$
0.011	$N^+(^3P) + N(4s^2P)1177$	0.125	$N(^4S^0) + N^+(^3D)1084$
0.093	$N^+(^3P) + N(3s^4P)8680$	0.008	$N(^4S^0) + N^+(3d^3F)5001$
0.043	$N^+(^3P) + N(3s^2D)1243$	0.010	$N(^4S^0) + N^+(3s^5P)630$
0.060	$N^+(^3P) + N(2p^4P)1134$	0.010	$N(^4S^0) + N^+(^3S)645$
0.032	$N^+(^3P) + N(3d^2D)1164$	0.011	$N(^4S^0) + N^+(3p^3D)5668$
		0.029	$N(^4S^0) + N^+(3p^3D)5681$
		0.093	$N(^4S^0) + N^{++}$

O_2 Excited state	Branching ratio	Dissociation products
$B\,^3\Sigma_u^-$	1.0	$O(^3P) + O(^1D)$
9.9 eV Peak	1.0	$O(^1D) + O(^1D)$
$A\,^3\Sigma_g^+$	1.0	$O(^3P) + O(^3P)$

Rydberg

Principle quantum number	Branching ratio	Dissociation product	Principle quantum number	Branching ratio	Dissociation product
	$X\,^2\pi_g$			$a\,^4\pi_u$	
$n=3$	1.0	$O(^3P) + O(^1D)$	$n=3$	0.5	$O(^1D) + O(^1S)$
$n=4$	1.0	$O(^3P) + O(^1S)$	$n=4$	0.5	$O(^3P) + O(3s^3S)1304$
$n\geq 5$	1.0	$O(^3P) + O(^1S)$	$n\geq 5$	0.68	$O(^3P) + O(3s^3S)1304$
	$A\,^2\pi_u$			$b\,^4\Sigma_g^+$	
$n=3$	0.5	$O(^1D) + O(^1S)$	$n=3$	0.5	$O(^3P) + O(3s^3S)1304$
$n=4$	0.5	$O(^3P) + O(3s^5S)1356$	$n=4$	0.5	$O(^3P) + O(3s\,^2S)1304$
$n\geq 5$	0.68	$O(^3P) + O(3s^5S)1356$	$n\geq 5$	0.68	$O(^3P) + O(3p^3P)8477$

TABLE IV (*Continued*)

Rydberg					
Principle quantum number	Branching ratio	Dissociation product	Principle quantum number	Branching ratio	Dissociation product
	$B\,^2\Sigma_g^-$			$c^4\Sigma_u^-$, $^2\pi$(III)	
$n=3$	0.5	$O(^3P)+O(3s^5P)1356$	$n=3$	0.5	$O(^3P)+O(3p^3P)8477$
$n=4$	0.5	$O(^3P)+O(3s^5P)7774$	$n=4$	0.5	$O(^3P)+O(3s^3P)879$
$n\geq 5$	0.68	$O(^3P)+O(3s^5P)7774$	$n\geq 5$	0.68	$O(^3P)+O(3s^3D)990$
	37 eV				
$n=3$	0.5	$O(^3P)+O(3s^5P)7774$			
$n=4$	0.5	$O(^3P)+O(4p^3P)4368$			
$n\geq 5$	0.68	$O(^3P)+O(4p^3P)4368$			

Ionization continua	Branching ratio	Dissociation products
$B\,^2\Sigma_g^-$	1.0	$O(^3P)+O^+(^4S^0)$
$c^4\Sigma_u^-$, $^2\pi$(III)	0.9	$O(^1D)+O^+(^4S^0)$
37 eV	0.7	$O(^3P)+O^+(^4P)$
	0.3	$O(^3P)+O^+(^2D)$

three or four major processes giving rise to various kinetic energy distributions of the dissociation fragments. Two of these processes have appearance potentials which correlate reasonably well with Franck–Condon thresholds for excitation of the $C\,^2\Sigma_u^+$ and $D\,^2\pi_g$ states of N_2^+. There is evidence for predissociation of the $C\,^2\Sigma_u^+$ probably via a $^4\pi_u$ giving $N(^4S^0)+N^+(^3P)$ as the dissociation fragments. Also there is little evidence for the excitation of the $D\,^2\pi_g$ state by electron impact. Thus, the participation of these states is questionable. However, in the absence of a better understanding, we have assigned the thresholds of Table II and dissociation fragments of Table IV to these processes. A third major process correlates with an appearance potential of about 35 eV[51,52] although there appears to be a range of possible appearance potentials for the higher kinetic energy dissociation fragments. In view of this, we have chosen an approximate threshold energy of 40 eV for the multitude of processes occurring in this range. The apportionment of the oscillator strengths among these processes is made to give a total dissociative ionization cross section in reasonable agreement with Rapp *et al.*[34] The relative contribution for each process is determined to preserve the approximate proportion of dissociation fragments as estimated from Deleanu and Stockdale[52] at 160 eV.

As a check on the 40 eV proportion, empirical determinations of the cross sections for dissociative ionization followed by radiative emission from N I and N II terms were summed. The thresholds for the onset of dissociative ionization appear clearly in many of the N I emission cross section measurements and allow an estimation of the size of the lower lying processes. These have been subtracted to give an estimate of the dissociative ionization contribution. The sum of these cross sections at 120 eV plus the cross section for production of N^{2+} as measured by Crow and McConkey[53] was found to agree with the previous determination to within 10%. Owing to the large number of N I emission cross sections which have been measured, this agreement would appear to add some credence to our assignment. Branching ratios within the 40 eV state have been assigned as shown in Table IV which give good agreement with the measured emission cross sections.

In Fig. 7 we show a comparison of the total N_2 dissociation cross section from Winters[35] with the "effective" dissociation cross section solid line obtained from the branching ratio assignments of Table IV. We also show a comparison of the computed dissociative ionization cross section with that of Rapp *et al.*[36] The agreement is generally good.

B. Oxygen

In contrast with N_2, O_2 is found to be less strongly bound. Here excitation to the repulsive wall above the

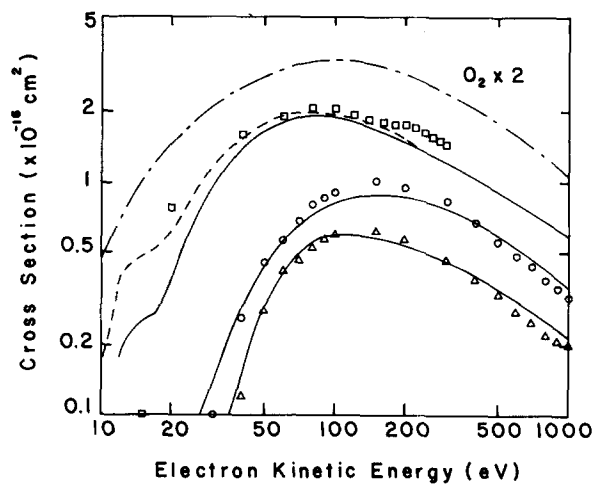

FIG. 7. Comparison of total dissociative cross section in N_2 from Winters[35] (□) with calculated cross sections (—) from branching ratios in Table IV. Also shown are the dissociative ionization cross sections in N_2(Δ) and O_2(○) measured by Rapp *et al.*[36] and our computed results N_2(—) and O_2(—).

dissociation limit and excitation of purely repulsive states appears to be the major cause of dissociation. Predissociation, however, does appear to play some role in the dissociation of O_2. Again as in N_2, however, dissociation is not a "new" process competing with direct excitation of the molecule but must again be treated in terms of branching ratios.

The main dissociation mechanism of O_2 below about 9.5 eV is the excitation to the repulsive wall of the $B\,^3\Sigma_u^-$ state. In addition to this major mechanism, predissociation of various vibrational levels of the $B\,^3\Sigma_u^-$ is also observed.[54] Considering the overwhelming strength of the continuum, we have set the branching ratio for dissociation at 1. The dissociation fragments are assigned to be $O(^3P)+O(^1D)$ as shown in Table IV. We have assumed the same dissociation branching ratio for the 9.9 eV state with dissociation fragments $O(^1D)+O(^1D)$. The $A\,^3\Sigma_u^+$ state is also assigned a branching ratio of 1 for dissociation in accord with results of Moore.[55] The dissociation fragments are assumed to be $O(^3P)+O(^3P)$.

The absorption spectrum of O_2 is extremely complex in the region from about 12 to 16 eV. The Rydberg series converging on the $a\,^4\pi_u$ and $A\,^2\pi_u$ states of O_2^+ autoionize[56,57] and predissociate.[49] Owing to this complexity, the Rydberg series lying in this interval have been treated using the same systematics as previously discussed for N_2 and the results are shown in Table IV.

Some measurements for the cross section for O I emissions in connection with O_2 excitation have been determined[58] although they are not as extensive as for N I. We have assigned the branching ratios appearing in Table IV to be in agreement with these cross sections where possible. The cross section for $O(^5S^0)$ and $O(^3S^0)$ is expected to be about the same size.[58d] States below the threshold for $O(^5S^0)+O(^3P)$ production are arbitrarily assigned following the same procedure as in N_2. While these results are approximate, they should give a reasonable clue as to what happens in this region. Extensive Rydberg series are observed leading to the $B\,^2\Sigma_g^-$ state. The absence of allowed transitions and diffuseness of the series in absorption suggest predissociation and autoionization occurs here.[59] Similar behavior is observed in the Rydberg series converging to the $c\,^4\Sigma_u^-$ state.[54] We again have used the systematics as applied to N_2 to arrive at the predissociation branchratios as given in Table IV. The dissociation fragments are expected to be triplet and quintet states of the oxygen atom.[49]

There is a somewhat better understanding of the processes leading to dissociative ionization of O_2[49,52,60] and there appear to be four major contributing processes. For the present purposes we will neglect the finer details[60] and attempt to be generally consistent with the gross features. The lowest peak in the kinetic energy distribution of O^+ atoms[52] and high Rydberg O atoms[49] correlates well with the $B\,^2\Sigma_g^-$ state (although see the discussion of Ref. 60). The absence of allowed emission $B\,^2\Sigma_g^- - A\,^2\pi_u$ suggests predissociation[49] and this has been recently established in photoelectron–photoion coincidence.[61] We have assumed the predissociation branching ratio is 1. The dissociation fragments are assumed to be $O(^3P)$ and $O^+(^4S^0)$. The 2.0 and 3.0 eV kinetic energy peaks of O^+ peaks[52] and high Rydberg atoms[49] have been attributed to predissociation of the $c\,^4\Sigma_u^-$ and $^2\pi_u$(III) states in O_2^+. There is, however, an observed $c\,^4\Sigma_u^- \rightarrow b\,^4\Sigma_g^-$ Hopfield system of O_2^+. In our analysis these states have been combined as an effective state with the branching ratio for predissociation and fragments given in Table IV. The 5 eV feature of O^+[52] and high Rydberg atoms[49] has been attributed to predissociation of the $^2\Sigma_g^-$ and/or $^4\Sigma_g^-$.[49] The dissociation fragments are expected to be $O(^3P)+O^+(^4P)$. The continuum oscillator strength has been apportioned between these three levels to give good agreement with the dissociative ionization cross section of Rapp *et al.* and to preserve our estimates of the relative contribution that each of these processes makes to the kinetic distribution of O^+ ions measured by Deleanu and Stockdale[52] at 85 eV.

Results of the branching ratio determinations for O_2 are shown in Fig. 7 where we show a comparison of the empirical and calculated dissociative ionization cross section. We also show our estimate of the total dissociation cross section in O_2 as determined from our branching ratios and cross sections (– · – line).

IV. RESULTS

The cross sections of Sec. II have been incorporated into a detailed atomic cross section approach to proton energy deposition. This method has been described in detail elsewhere[16–18] and only a brief review will be given here. In the continuous slowing down approximation (CSDA) the loss function or stopping power, $L(E)$, is given by

$$L(E) = -(1/n)(dE/dx) \tag{17}$$

where n is the gas density and dE/dx is the rate of change of the incident particle's kinetic energy with distance between x and $x+dx$. The loss function is constructed from

$$L(E) = \sum_i \rho_i L^i(E) \tag{18}$$

where i runs over the number of gases contributing to the loss function and ρ_i is the fractional composition of the ith constituent. Each gas constituent loss function for the proton deposition problem is obtained from

$$L^i(E) = \sum_{c=0}^{1} f^c \left[\sum_d w_d \sigma_d^c + \sum_I (W_I + \langle T_I^c \rangle)\sigma_I^c + L_{\text{elas}} \right], \tag{19}$$

where c is the charge state of the projectile ($c=0$ is hydrogen and $c=1$ is a proton), d runs over the number of discrete processes with threshold energy w_d and cross section σ_d^c, I runs over all continuous processes with threshold W_I and mean energy loss to the continuum $\langle T_I^c \rangle$ with total cross section σ_I^c and L_{elas} is the elastic loss. In Eq. (19) f^c is the equilibrium fraction for charge component c of the beam, and for a multiconstituent gas we define this quantity by

$$f^1 = \left[\sum_i \rho^i \sigma_{01}^i \Big/ \sum_i (\rho^i \sigma_{01}^i + \rho^i \sigma_{10}^i) \right]$$

$$f^0 = 1 - f^1 ,$$

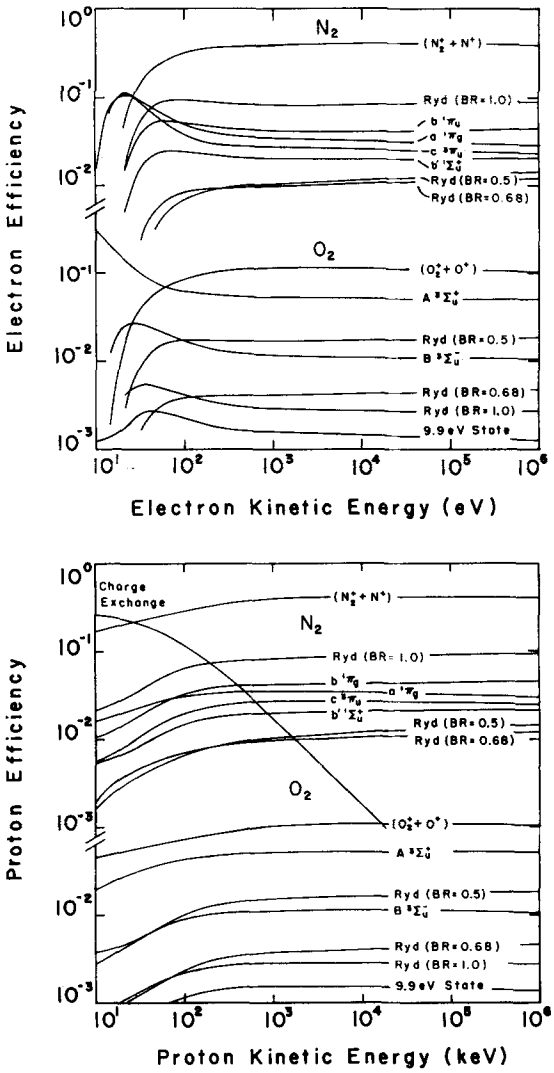

FIG. 8. (a) Electron efficiencies for important atom producing states. Rydberg levels are summed for the same branching ratio values. (b) Proton efficiencies for important atom producing states. Rydberg levels are summed as above.

where σ_{01}^{i} is the stripping cross section for constituent i and σ_{10}^{i} is the capture cross section for constituent i. While the spatial aspects of the energy deposition can be simply obtained in CSDA, we wish to concentrate here on the efficiency or fraction of the incident projectile's kinetic energy which is eventually deposited in each state of excitation of the gas. The efficiency is defined by

$$\mathrm{Eff}(E) = [W_k J_k(E)/E] ,$$

where J_k is the total number of excitations of the state K which result in degrading to zero energy the incident projectile of kinetic energy E and *all* subsequent electrons produced. It is composed of three contributions

$$J_k = J_{k,\,\mathrm{protons}} + J_{k,\,\mathrm{hydrogen}} + J_{k,\,\mathrm{electrons}} .$$

In Fig. 8 we show electron impact efficiences for excitation of important atom producing states in N_2 and O_2. Also shown for comparison is the total efficiency for the production of ions $(N_2^+ + N^+)$ and $(O_2^+ + O^+)$. In Fig. 8 we also show the heavy particle impact efficiencies that we obtain for important atom producing states in N_2 and O_2. Of interest here is the increasing importance of the charge exchange cycle as a mode of energy loss below 10 MeV. As the efficiency for the charge exchange cycle increases there is a compensating change in the efficiencies of other states. The leveling off of the efficiencies above about 10 MeV is not expected to continue to energies above about 1 GeV, since nuclear processes will begin to play a significant role in the energy loss. In Fig. 9, we show our electron and proton eV/ion pair as a function of energy. We also show our calculated eV/atomic species in N_2 and O_2 as a function of energy.

It is to be noted that atomic oxygen is produced almost as efficiently as atomic nitrogen even though the abundance of O_2 in air is only one quarter as great as N_2. As can also be clearly seen, the eV/atomic species is a rapidly changing function of energy below about 150 eV in the case of electron impact and 500 keV in the case of proton impact. The eV/ion pair in air for electron impact is 34.5 at 10^4 eV while for proton impact at 2 MeV it is 35.8. The combination of these results gives ~ 1.27 N and N^+ atoms produced per ion pair in air at high energy (in the asymptotic region) for both proton and electron impact. This result is ~ 27% larger than the value used by Nicolet.[1] It is in good agreement with the value used by Ruderman and Chamberlain[2] and about 15% smaller than that used by Crutzen *et al.*[3] We obtain a value ~ 1.15 O and O^+ atoms produced in air per ion pair by electron or proton impact at high energy. This is the first reported value for the atomic oxygen production by electron and proton impact to our knowledge. It is interesting to note that the eV/oxygen atom ratio declines for lower electron energy. This is a consequence of the large production of oxygen atoms from the $A\,^3\Sigma_g^+$ state.

Our results are summarized in Table V. We have listed approximate proportions of excited atoms neglecting cascade to the lowest allowed term. While these

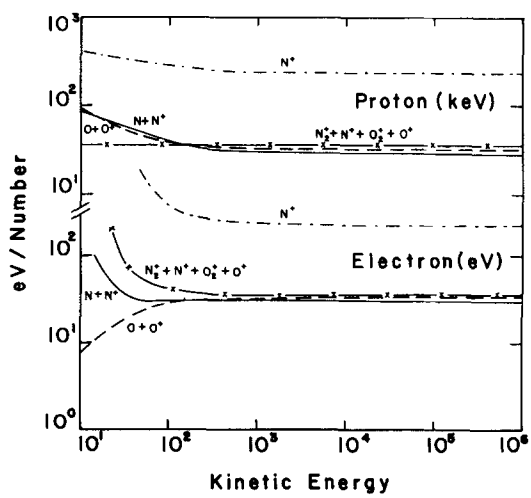

FIG. 9. eV/ion pair (-x-x); eV/atomic nitrogen species (—); eV/N^+(- · - · -); eV/atomic oxygen species (----). Upper curves, protons (kinetic energy in keV); lower curves, electrons (kinetic energy in eV).

TABLE V. Distribution of states of atomic nitrogen produced by proton impact at 1 MeV.

Species	eV/species	Number/ion pair
$N(^4S^0)$	6.67×10^1	0.538
$N(^2D^0)$	9.43×10^1	0.381
$N(^2P^0)$	4.62×10^2	0.078
$N(3s^2P)$	2.09×10^3	0.018
$N(3s^4P)$	1.66×10^3	0.022
$N(3s^2D)$	6.39×10^3	0.56×10^{-2}
$N(4s^2P)$	1.05×10^5	0.34×10^{-3}
N^+	2.33×10^2	0.154
Total ground state N atoms		= 0.538/ion pair
Total excited state N atoms		= 0.660/ion pair
Total atom production (1 MeV)		= 1.2/ion pair
Total atom production (asymptotic)		= 1.27/ion pair

proportions are to some degree arbitrary, they should serve as useful estimates until more detailed empirical or theoretical results become available.

To gain a feeling for the sensitivity of the nitrogen atom production on the low energy portion of the spectrum ($\leq$ 30 eV), where our "effective" cross section determined from our branching ratio assignments is in poorest agreement with experiment we have arbitrarily set the $a\,^1\pi_g$ branching ratio equal to unity. The resulting dissociation cross section is shown as a dashed line in Fig. 7. Using this $a\,^1\pi_g$ branching ratio, the asymptotic eV/atom nitrogen ratio drops to ~25.0 or 1.42 N and N^+ atoms/ion pair. Thus a factor of 5 change in the branching ratio for the $a\,^1\pi_g$ results in only about an 11% change in the eV/atom ratio. Because of the large population of this state, it has the largest influence of any state considered for the eV/nitrogen atom ratio. Consequently, the atom production rates are surprisingly insensitive to the low energy cross section behavior. In view of the relatively large uncertainties of the total dissociation cross section measurement of Winters,[35] we feel the 1.27 N or N^+ atoms/ion pair is a "best" estimate.

V. SUMMARY AND CONCLUSIONS

We have used well founded theoretical prescriptions to extrapolate proton and electron cross sections into the relativistic domain. Since both the high and low energy behavior of the cross section forms is required for practical considerations we have found appropriate analytic forms which span the range from threshold to relativistic energies. These cross sections combined with branching ratios for dissociation (or alternately emission and autoionization) form a self-consistent description of the energy deposition process.

We have used these results to arrive at the relativistic eV/ion pair for electrons and protons as well as the eV/atomic species. In addition we have obtained some estimate as to the proportion of excited atoms to ground state atoms. Finally, it is observed that the efficiency for production of atomic species changes with the particle energy.

ACKNOWLEDGMENTS

This work was sponsored in part by NASA Grant NGL 10-005-008.

[1]M. Nicolet, Planet. Space Sci. **23**, 637 (1975).
[2]M. A. Ruderman and J. W. Chamberlain, Planet. Space Sci. **23**, 247 (1975).
[3]P. J. Crutzen, I. S. A. Isaksen, and G. C. Reid, Science **189**, 457 (1975).
[4]A. E. S. Green, and C. A. Barth, J. Geophys. Res. **70**, 1038 (1965).
[5]A. E. S. Green, and C. A. Barth, J. Geophys. Res. **72**, 3975 (1967).
[6]L. R. Peterson, S. S. Prasad, and A. E. S. Green, Can. J. Chem. **47**, 1774 (1969).
[7]A. E. S. Green, S. S. Prasad, and L. R. Peterson, NASA Spec. Publ. SP-**305**, 91 (1972).
[8]R. S. Stolarski, V. A. Dulock, C. E. Watson, and A. E. S. Green, J. Geophys. Res. **72**, 3953 (1967).
[9]E. C. Watson, V. A. Dulock, R. S. Stolarksi, and A. E. S. Green, J. Geophys. Res. **72**, 3961 (1967).
[10]P. B. Abraham, K. A. Brunstein, and T. L. Cline, Phys. Rev. **150**, 1088 (1966).
[11]K. P. Beuerman, J. Geophys. Res. **76**, 4291 (1971).
[12]H. Bethe, Z. Phys. **76**, 293 (1932).
[13]H. Bethe, in *Handbuch der Physik*, edited by H. Geiger and K. Scheel (Springer, Berlin, 1933), Vol. 24/1, p. 273.
[14]M. Inokuti, Rev. Mod. Phys. **43**, 297 (1971).
[15]A. E. S. Green and R. J. McNeal, J. Geophys. Res. **76**, 133 (1971).
[16]J. H. Miller, and A. E. S. Green, Radiat. Res. **54**, 343 (1973).
[17]B. C. Edgar, W. T. Miles, and A. E. S. Green, J. Geophys. Res. **68**, 6595, 1973.
[18]B. C. Edgar, H. S. Porter, and A. E. S. Green, Planet. Space Sci. **23**, 787 (1975).
[19]H. W. W. Massey, and C. B. O. Mohr, Proc. R. Soc. London Ser. A **140**, 613 (1933).
[20]R. A. Berg and A. E. S. Green, Adv. Quantum Chem. **7**, (1973).
[21]P. A. Kazaks, P. S. Ganas, and A. E. S. Green, Phys. Rev. A **6**, 2169 (1972).
[22]S. M. Silverman, and E. N. Lassettre, J. Chem. Phys. **42**, 3420 (1965).
[23]S. M. Silverman and E. N. Lassettre, J. Chem. Phys. **40**, 2922 (1964).
[24]C. Moller, Ann. Phys. **14**, 531 (1932).
[25]H. J. Bhabha, Proc. R. Soc. London Ser. A **164**, 257 (1938).
[26]C. B. Opal, E. C. Beaty, and W. K. Peterson, At. Data **4**, 209 (1972).
[27]A. E. S. Green, and T. Sawada, J. Atmos. Terr. Phys. **34**, 1719 (1972).
[28]D. Rapp and P. Englander-Golden, J. Chem. Phys. **43**, 5 (1965); see also L. J. Kieffer and G. H. Dunn, Rev. Mod. Phys. **38**, 1 (1966).
[29]B. L. Schram, F. J. deHerr, M. J. van der Wiel, and J. Kistemarker, Physica (Utrecht) **31**, 94 (1965).
[30]N. F. Mott and H. S. W. Massey, *The Theory of Atomic Collisions*, 3rd edtn. (Oxford University, London, 1965).
[31]J. B. Crooks and M. E. Rudd, Phys. Rev. A **3**, 1628 (1971); M. E. Rudd (personal communication).
[32]L. H. Tobunre (personal communication, 1973).
[33]S. P. Khare, Planet. Space Sci. **17**, 1257 (1969).
[34]S. C. Soong, *Inner Shell Contributions to Electron Degradation Spectra* (1976).
[35]H. F. Winters, J. Chem. Phys. **44**, 1472 (1966).
[36]D. Rapp, P. Englander-Golden, and D. Briglia, J. Chem. Phys. **42**, 4081 (1965).
[37]L. S. Polak, D. I. Slovetskii, and A. S. Sokolov, High Energy Chem. **6**, 350 (1972).
[38]A. Lofthus, Can. J. Phys. **35**, 216 (1957).

[39]A. E. Douglass and G. Herzberg, Can. J. Phys. **29**, 294 (1951).
[40]D. E. Shemansky, J. Chem. Phys. **51**, 5487 (1969).
[41]R. W. Nicholls, J. Phys. B **1**, 1192 (1968).
[42]P. K. Carrol and R. S. Mulliken, J. Chem. Phys. **21**, 2243 (1954).
[43]R. N. Zare, E. O. Larsson, and R. A. Berg, J. Mol. Spectrosc. **15**, 117 (1965).
[44]P. K. Carroll and C. P. Collins, Can. J. Phys. **47**, 563 (1969).
[45]K. Dressler, Can. J. Phys. **47**, 547 (1969).
[46]P. K. Carroll and K. Yoshino, J. Chem. Phys. **47**, 3073 (1967).
[47]E. C. Zipf, Trans. Amer. Geophys. Union **55**, 363 (1974).
[48]G. R. Cook and M. Ogawa, Can. J. Phys. **43**, 256 (1965).
[49]R. S. Freund, J. Chem. Phys. **54**, 3125 (1971).
[50](a) M. J. Mumma and E. C. Zipf, J. Chem. Phys. **55**, 5582 (1971); (b) J. M. Ajello, J. Chem. Phys. **53**, 1156 (1970); (c) J. M. Arts and F. J. deHerr, J. Chem. Phys. **52**, 45 (1971).
[51]K. C. Smyth, J. A. Schiavone, and R. S. Freund, J. Chem. Phys. **59**, 5225 (1973).
[52]L. Deleanu and J. A. Stockdale, Oak Ridge Nat. Lab. ORNL-TM-4909 (1975).
[53]A. Crowe and J. W. McConkey, J. Phys. B **6**, 2108 (1973).
[54]P. M. Krupenie, J. Phys. Chem. Ref. Data **1**, 423 (1972).
[55]J. H. Moore, Jr., J. Geophys. Res. **77**, 5567 (1972).
[56]G. R. Cook, and R. H. Metzger, J. Chem. Phys. **41**, 321 (1964).
[57]A. J. Blake, and J. H. Carver, J. Chem. Phys. **47**, 1038 (1967).
[58](a) W. L. Borst and E. C. Zipf, Phys. Rev. A **4**, 153 (1971); (b) W. Sroka, Z. Naturforsch. Teil A **23**, 2004 (1968); (c) J. M. Ajello, J. Chem. Phys. **55**, 3156 (1971); (d) G. M. Lawrence, Phys. Rev. A **2**, 397 (1970); (e) M. J. Mumma and E. C. Zipf, J. Chem. Phys. **55**, 1661 (1971); (f) J. F. M. Arts and F. J. deHerr, Physics **56**, 294 (1971).
[59]K. Yoshino and Y. Tanaka, J. Chem. Phys. **48**, 4859 (1968).
[60]J. Schopman, and R. Locht, Chem. Phys. Lett. **26**, 596 (1974).
[61]C. J. Danby, and J. H. Eland, Int. J. Mass Spectrom. Ion. Phys. **8**, 143 (1972).
[62]R. J. McNeal and D. C. Clark, J. Geophys. Res. **74**, 5065 (1969).
[63]F. J. deHerr, J. Schulten, and H. Monstafa, Physica (Utrecht) **32**, 1766 (1966).
[64]J. W. Hooper, D. S. Harmer, D. W. Martin, and E. W. McDaniel, Phys. Rev. **125**, 3000 (1962).